Volume 15 | Number 7 | 7 April 2015 | Pages 1621–1784

Lab on a Chip

Miniaturisation for chemistry, physics, biology, materials science and bioengineering

www.rsc.org/loc

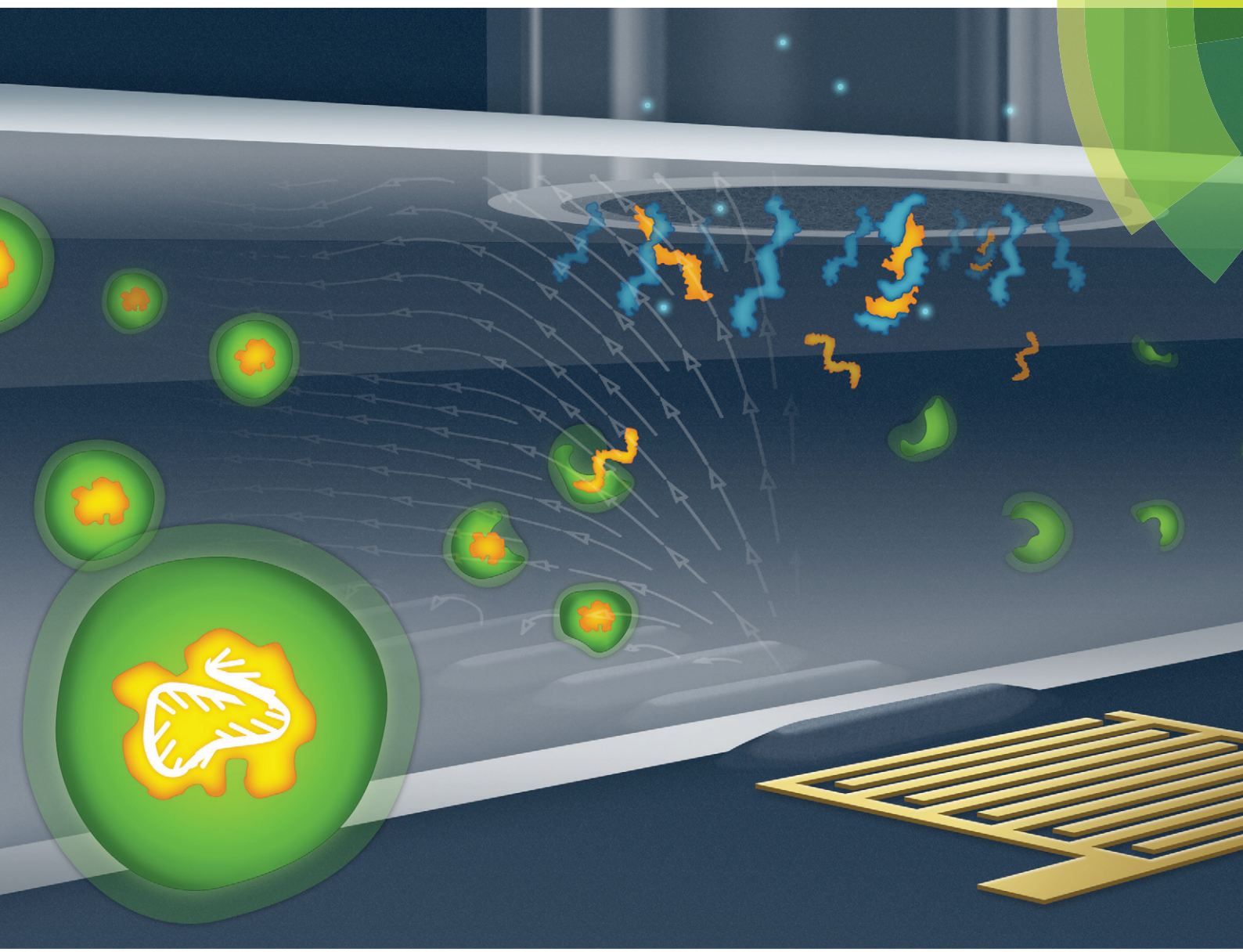

ISSN 1473-0197

ROYAL SOCIETY OF CHEMISTRY

PAPER

David B. Go, Hsueh-Chia Chang *et al.*

On-chip surface acoustic wave lysis and ion-exchange nanomembrane detection of exosomal RNA for pancreatic cancer study and diagnosis

Lab on a Chip

PAPER

View Article Online
View Journal | View Issue

Published on 11 February 2015. Downloaded by University of Notre Dame on 20/03/2015 19:26:49.

Cite this: *Lab Chip*, 2015, **15**, 1656

On-chip surface acoustic wave lysis and ion-exchange nanomembrane detection of exosomal RNA for pancreatic cancer study and diagnosis†

Daniel Taller,[ab] Katherine Richards,[c] Zdenek Slouka,[bd] Satyajyoti Senapati,[bd] Reginald Hill,[c] David B. Go*[ad] and Hsueh-Chia Chang*[bd]

Received 9th January 2015,
Accepted 11th February 2015

DOI: 10.1039/c5lc00036j

www.rsc.org/loc

There has been increasing evidence that micro and messenger RNA derived from exosomes play important roles in pancreatic and other cancers. In this work, a microfluidics-based approach to the analysis of exosomal RNA is presented based on surface acoustic wave (SAW) exosome lysis and ion-exchange nanomembrane RNA sensing performed in conjunction on two separate chips. Using microRNA hsa-miR-550 as a model target and raw cell media from pancreatic cancer cell lines as a biological sample, SAW-based exosome lysis is shown to have a lysis rate of 38%, and an ion-exchange nanomembrane sensor is shown to have a limit of detection of 2 pM, with two decades of linear dynamic range. A universal calibration curve was derived for the membrane sensor and used to detect the target at a concentration of 13 pM in a SAW-lysed sample, which translates to 14 target miRNA per exosome from the raw cell media. At a total analysis time of ~1.5 h, this approach is a significant improvement over existing methods that require two overnight steps and 13 h of processing time. The platform also requires much smaller sample volumes than existing technology (~100 μL as opposed to ~mL) and operates with minimal sample loss, a distinct advantage for studies involving mouse models or other situations where the working fluid is scarce.

1. Introduction

Early detection of pancreatic cancer is critical to improving long term survival rates, which are currently less than 6% within 5 years of diagnosis.[1] Traditionally, the presence of a malignant tumor is confirmed upon biopsy procurement—an invasive procedure, which in itself is not useful for early detection since most patients develop symptoms only with late stage/metastatic disease. A minimally invasive method, which could be done on routinely collected biological samples, would be ideal for the diagnosis of pancreatic cancer and the subsequent tailoring of molecularly targeted therapies for patients.

MicroRNA (miRNA), in particular, have begun to receive significant attention as important indicators of cancer state and progression. MiRNAs are small strands (~22 nucleotides) of RNA that can be upregulated or downregulated in cancer cells and function as posttranscriptional gene regulators by binding to their target messenger RNAs (mRNAs). A number of recent findings have suggested that understanding miRNA regulation and expression is essential to understanding cancer development and could give an indication of disease presence before the onset of recognizable symptoms in the patient.[2–4] Furthermore, miRNAs are ideal biomarkers for early diagnosis of cancer due to their importance in disease development, their presence in biological fluids, and their short sequence length, which leads to increased stability. The miRNA transfer between cells in a tumor is mediated by exosomes, secreted membrane vesicles ~30–200 nm in diameter that are present in blood, saliva, urine, and other bodily fluids.[5–7] Therefore, the detection of miRNAs enclosed in exosomes is of great promise to the study and the non-invasive diagnosis of many cancers. Pancreatic cancer, as a particularly important but difficult to diagnose cancer, serves as a prime candidate for advances in exosome miRNA biomarker detection.

Extracting RNA from exosomes derived from extracellular biological matrices in sufficient concentration for conventional RNA detection methods such as reverse transcription polymerase chain reaction (RT-PCR) is not trivial, typically requiring multiple stages of ultra-centrifugation or field-flow fractionation.[8–10] In total, the typical standard process

[a] *Department of Aerospace and Mechanical Engineering, University of Notre Dame, Notre Dame, Indiana 46556, USA. E-mail: dgo@nd.edu*
[b] *Center for Microfluidics and Medical Diagnostics, University of Notre Dame, Notre Dame, Indiana 46556, USA. E-mail: hchang@nd.edu*
[c] *Department of Biological Sciences, University of Notre Dame, Notre Dame, Indiana 46556, USA*
[d] *Department of Chemical and Biomolecular Engineering, University of Notre Dame, Notre Dame, Indiana 46556, USA*

† Electronic supplementary information (ESI) available. See DOI: 10.1039/c5lc00036j

This journal is © The Royal Society of Chemistry 2015

Published on 11 February 2015. Downloaded by University of Notre Dame on 20/03/2015 19:26:49.

requires two overnight steps and approximately 13 h of processing time, demanding the use of multiple instruments and a wide variety of chemical kits and washes, with training times and other common inefficiencies frequently leading to several days in processing time. Additionally, these methods typically require large starting volumes of biomaterial, *e.g.*, 5–10 mL of cell culture, to collect a sufficient number of exosomes required for RT-PCR analyses due to exosome loss during the isolation process. Therefore, an on-chip device with low losses and reduced processing times would expedite cancer cell culture and animal studies and human cancer diagnostics.

In order to overcome the aforementioned obstacles, a new on-chip analysis strategy has been developed for the rapid lysis of exosomes and the detection of the miRNA released from these exosomes. Two microfluidic platforms are developed here, a lysis device and a separate detection device. The two devices reduce the total analysis time to ~1.5 h, which includes ~30 min for lysing and ~1 h for detection. The smaller sample volume required in the present study, ~100 μL, makes this platform more attractive for studies where only small amounts of biological fluid, *e.g.*, blood, can be safely extracted as would be the case in mouse models. This would also be ideal for use with fine needle aspiration (FNA) samples from clinical patients; a technique routinely conducted to confirm cancer diagnosis by pathological verification of neoplastic cells. The scientific community could gain much more insight about the tumor from fluid collected during this procedure, but the total sample volume is very limited, with only 250–500 μL of fluid typically being collected with each FNA.[11,12] Although the study presented herein was conducted with cancer cell media, a recent study conducted by Schageman *et al.*[6] shows that both the total exosome count and the concentration of exosomal RNA are greater in blood serum derived from human donors than in cell media samples, implying that studies involving human-derived samples should be feasible using the given approach.

1.1 Overview of lysis and detection devices

Lysis is achieved *via* surface acoustic waves (SAWs), which are Rayleigh waves generated on the surface of a piezoelectric crystal by alternating current applied through an interdigitated electrode transducer.[13,14] When the SAW waves interact with a bulk liquid droplet or film, as depicted in Fig. 1a, scattered sound waves produce an acoustic pressure in the liquid bulk while the electric component of the wave produces an electric Maxwell pressure at the solid liquid interface.[15,16] Historically, SAWs have been used in the electronics industry as filters, oscillators, convolvers, and transformers.[13,17] More recently, SAW devices have found new life in the microfluidics discipline as a tool to overcome the traditional microscale challenges of constrained geometries, surface tension, and viscous effects in order to provide high Reynolds number flows. In particular, it has been shown that SAWs on the surface of the piezoelectric crystal will scatter into a liquid bulk, inducing an acoustic radiation force which allows Reynolds numbers as high as 7000 and effective turbulent mixing.[18] In addition, the electromechanical coupling inherent in SAWs produces an electric field as high as ~10^6 V m^{-1} at the surface of the substrate.[15,19] The application of both the electric and acoustic pressures applied by SAWs have proven useful for focusing and sorting particles and cells,[20,21] for producing charged aerosols for mass spectrometry,[15,22] and for cell lysis.[23,24] In this work, we utilize SAWs to lyse exosomes, which are an order of magnitude smaller than most cells. The lysis of particles as small as exosomes is likely made possible due to the effects of the acoustic radiation

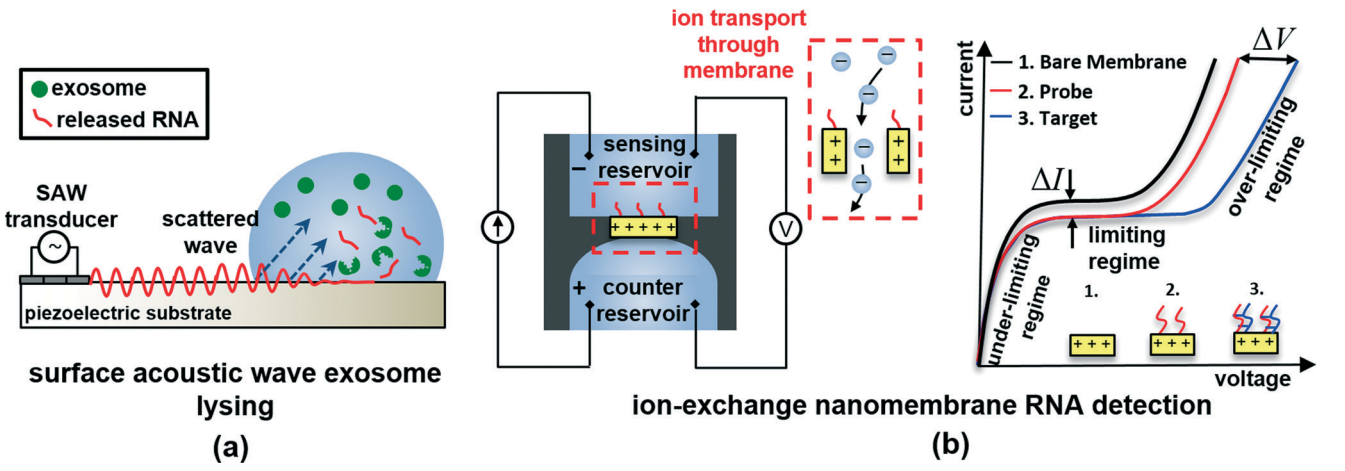

Fig. 1 (a) Schematic of surface acoustic wave (SAW) device (side view) and SAW-induced lysing of exosomes to release RNA for detection. SAWs generated at the transducer refract into the liquid bulk, inducing fluid motion, and electromechanical coupling also generates a complimentary electric wave at the surface of the substrate. (b) Schematic of ion-exchange nanomembrane sensor consisting of two reservoirs separated by the membrane. RNA in the sensing reservoir hybridize to complimentary oligos immobilized on the surface of the membrane. The inset shows the ion transport through the device to generate current and the right image is a characteristic current–voltage curve illustrating the under-limiting, limiting, and over-limiting regimes.

Published on 11 February 2015. Downloaded by University of Notre Dame on 20/03/2015 19:26:49.

force and the dielectrophoretic force acting on small particles, as detailed in previous studies on SAW-induced particle manipulation.[25–28] The well-known dielectrophoretic force arises due to an induced particle dipole occurring in an inhomogeneous electric field. The acoustic radiation force is analogous, with a gradient in mechanical stress replacing the electric field gradient as the mechanism and factors involving the relative density and compressibility of the particle and the surrounding medium replacing similar factors involving the relative electric permittivity and conductivity. SAW lysis thus proves to be an excellent alternative to traditional chemical or surfactant lysates,[29–31] which can interfere with RNA detection downstream by changing the buffer pH and ionic strength or forming/disrupting self-assembled layers for surface assays.

Label-free, specific on-chip detection of RNA is achieved by using a separate device, an ion-exchange nanomembrane sensor developed by the authors' group.[32–34] The sensor consists of an anion-exchange nanoporous membrane sandwiched between two reservoirs of fluid, as shown in Fig. 1b. When an electric current is applied across the membrane, anions are driven through the membrane pores, producing a corresponding voltage drop measured across the membrane. Measuring the current–voltage characteristic (CVC), which has been the subject of extensive study,[34–36] thus becomes the basis for RNA detection. Briefly, the CVC of the nanomembrane consists of three regimes as illustrated in Fig. 1b: an ohmic under-limiting regime at low voltages, a limiting regime where current saturates at intermediate voltages, and an over-limiting regime at high voltages where current once again increases abruptly. It has been shown that the CVC dramatically changes when large, negatively charged molecules such as RNA are adsorbed to the surface of the positively charged membrane.[34] In particular, the over-limiting regime shifts rightward to higher voltages as more molecules adsorb to the surface, as shown by the voltage shift ΔV in Fig. 1b. The sensor works on the principle that after oligonucleotide probes are functionalized on the surface of the membrane, target RNA bind to the surface selectively while non-target molecules do not, allowing the target RNA concentration to be accurately determined through CVC measurements. Building on previous work that has demonstrated this detection method for solutions of pure DNA and RNA dissolved in phosphate buffer saline (PBS),[34] in this work we perform membrane sensor detection of RNA suspended in cell media for the first time. Together, these two separate devices provide a complete platform for the detection of exosomal RNA for pancreatic cancer study and diagnosis.

2. Materials and methods

2.1 Target miRNA and oligonucleotide probe

As our initial target, we focused on the miRNA hsa-miR-550-002410 (miR-550, base sequence given by AGUGCCUGAGGGAGUAAGAGCCC), which is known to be present in pancreatic exosomes and which early reports suggest may be an indicator for cancer development.[37] Target miRNA were extracted from exosomes in cell media from the PANC1 cell line. PANC1 cells were grown in the initially exosome-free Dulbecco's Modified Eagle's Medium (Sigma Aldrich), with the exosome-containing media being collected once 70–90% confluent. In addition, artificial target miRNA were purchased (Life Technologies) to serve as a baseline during calibration, diluted to known concentrations with UltraPure™ DNase/RNase-Free distilled water (Invitrogen). PBS 10× solution with pH 7.4 was purchased from Hoefer and diluted to 0.1× for current–voltage measurements with the membrane sensor and to 4× concentration to wash the membrane to prevent non-specific binding. For RNA detection, an amine-coupled ssDNA oligionucleotide probe of the same length as the miR-550 target and with a complementary sequence of TCACGGACTCCCTCATTCTCGGG was also purchased (Life Technologies).

2.2 Surface acoustic wave (SAW) device integrated into microfluidic channel

The SAW device was fabricated using standard UV photolithographic methods. Twenty pairs of titanium/aluminum interdigitated electrodes (Ti/Al 20 nm/200 nm) were patterned on a 127.68° *yx*-cut piezoelectric lithium niobate ($LiNbO_3$) substrate (Precision Micro-Optics PWLN-431232) to form an electrode-width controlled (EWC) single phase unidirectional SAW transducer (SPUDT), which generates plane SAWs propagating in one direction only.[38,39] Each SAW device consisted of a rectangular piece of $LiNbO_3$ 16 mm × 40 mm and 0.5 mm in thickness. The fingers of the interdigitated electrodes spanned 4 mm in length and were designed to produce a SAW wavelength of 136 μm, with finger width and spacing based on multiples of 1/8 of the wavelength as determined according to standard EWC SPUDT design.[38,40–42] The operating frequency was 28.3 MHz. The SAW was activated by a function generator (Agilent 33250A) in series with an amplifier (E&I 325LA RF Power Amplifier).

A channel for fluid flow was fabricated using three layers of polycarbonate thermosoftening plastic. The channel and holes for the inlet and outlet were cut and sealed together *via* heat curing in a manner similar to Slouka *et al.*,[32] yielding a channel with height of 300 μm and width of 2000 μm. The channel was constructed with an opening in the bottom and the front side, so that it conformed to the size of the $LiNbO_3$ substrate on which the SAW electrodes were fabricated. The channel was then attached to the substrate with UV curing glue (Loctite 3492) and cured (Electro-Cure 500 UV Flood Curing Chamber). The open channel facing the SAW device is sealed with UV curable glue (Acrifix 1R 0192) so that no fluid leaked out of the channel. The outlet was made out of Tygon tubing, while a port fitting cast out of polyurethane was attached to the inlet hole. The combined microfluidic channel and SAW lysis unit is shown in Fig. 2a and b.

Sample was pumped through the device at a rate of 250 μL h^{-1} and the SAW device operated at 1 W of power. The device was operated for 25 min. and the residence time in

 This journal is © The Royal Society of Chemistry 2015

Published on 11 February 2015. Downloaded by University of Notre Dame on 20/03/2015 19:26:49.

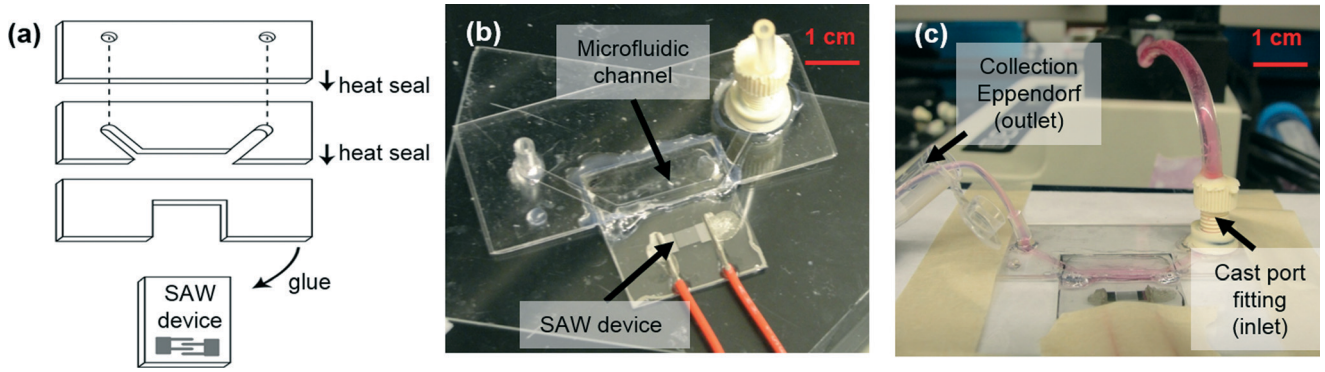

Fig. 2 (a) Schematic of SAW lysis device. (b)–(c) Images of the as-fabricated SAW device and liquid channel used to lyse exosomes.

the portion of the channel exposed to the SAW device was approximately 30 s. Sample was collected at the outlet of the microfluidic channel into an Eppendorf tube, as shown in Fig. 2c, before transfer to the nanomembrane sensor device *via* pipette.

Visualization and measurement of the particle distribution in the suspension before and after SAW exposure was conducted using light scattering-based particle tracking (Nanosight LM10). Unlike traditional dynamic light scattering (DLS) technology, a video is taken with the Nanosight so that particles may be counted individually and their Brownian motion can be recorded over time, yielding more accurate measurements of both particle size and concentration for the exosome sizes anticipated here (~100 nm). All samples measured with the Nanosight were diluted in 0.1× PBS to between 1×10^8 and 4×10^8 particles mL^{-1} to obtain maximum accuracy in the results, as prescribed in previous studies.[5,43] The Nanosight exosome concentration and size distribution statistics reported by the Nanosight, have been proven to yield accurate results for exosomes and thus the Nanosight is among the most widely-used and most reliable methods for *in vivo* exosome quantification available to researchers to date.[5,7,43–50]

2.3 Ion-exchange nanomembrane sensor

The ion-exchange nanomembrane device consisted of two reservoirs made of hard polyurethane resin bridged together by a heterogenous ion-exchange membrane (type AMH5E-HD RALEX® membrane, Mega a.s.) as illustrated in Fig. 1b. Two silicone reservoirs were cast from a two-component silicone RTV resin (TAP Plastic Inc.) in a silicone mold. The ion-exchange nanomembrane was sandwiched between the two silicone molds, and the system was filled with polyurethane resin (TAP Quik-Cast Polyurethane Resin, 1 : 1 ratio) and allowed to set for 30 minutes. Release of the silicone mold produced the membrane sensor chip. The membrane was cut with a razor blade to be just large enough to cover the exposed sensing area of 0.25 mm^2, with the probes attached to membrane surface as described in previous work.[34] The bottom reservoir was sealed with a plexiglass (Poly(methyl methacrylate) or PMMA) sheet with two holes for electrodes. The biological fluid sample was transferred to the membrane sensor after SAW lysis as described in the previous section.

For RNA detection, an amine-coupled oligionucleotide probe of the same length as the miR-550 target and with a complementary sequence was purchased from Life Technologies as previously noted. The process to attach the probe to the membrane using ethyl-3-(3-dimethylaminopropyl)-carbodiimide (EDC) and benzophenone-3,3′,4,4′-tetracarboxylic acid powders (Sigma Aldrich) has been detailed elsewhere.[34] To summarize, the surface was first treated with photo-reactive benzophenone-3,3′,4,4′-tetracarboxylic acid and exposed to UV light (Electro-Cure 500, Electro-Lite Corp.) in order to create COOH groups on the surface of the membrane, followed by treatment with 0.4 M EDC for 30 min. Lastly, an overnight incubation with the probe in 0.1× PBS solution was performed to covalently bind the probe to the membrane surface.

In order to perform detection of multiple samples on the same membrane sensor, a pH 13 solution of NaOH and 0.1× PBS was used to dehybridize the target RNA from the probes between runs. A wash with 4× PBS was used to wash away contaminants and to eliminate non-specific binding prior to each measurement. After application of the NaOH solution or the 4× PBS solution, repeated measurements were taken using a 0.1× PBS solution buffer until the CVC stabilized, a process which takes 5 to 15 min per measurement.

3. Results and discussion

3.1 Raw sample analysis

Prior to any processing of the cell media sample with our microfluidic devices, the cell media was spun down at 1500 rpm for 5 min and then analysed to confirm the presence of exosomes and the presence of the target miR-550. The presence of exosomes was confirmed using transmission electron microscopy (TEM) imaging, where Fig. 3a shows a representative TEM image of particles size ~20–50 nm, consistent with TEM analyses by other researchers.[51]

We also used RT-PCR to confirm that the target RNA was present in the sample. In brief, exosomes were collected from

Published on 11 February 2015. Downloaded by University of Notre Dame on 20/03/2015 19:26:49.

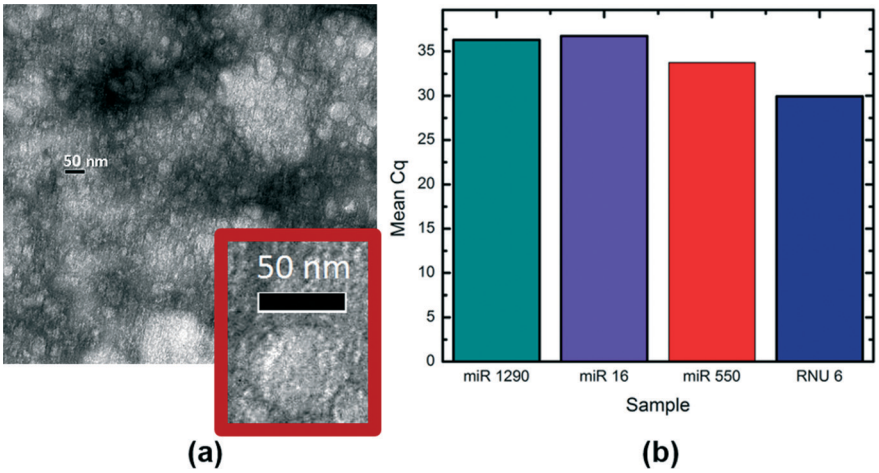

Fig. 3 (a) Representative transmission electron microscope (TEM) image, confirming the presence of exosomes in the ~30–50 nm size range in the sample. A zoomed-in view of a single exosome is shown in the inset. (b) Mean quantification cycle (Cq) for different RNA targets from RT-PCR analysis after chemical lysing.

an initial sample 10 mL cell media sample *via* the ExoQuick TC™ exosome precipitation solution and incubated at 4 °C overnight. The exosome pellet was then collected and chemically lysed (lysate Triton X-100 added to the solution at 2% by volume and incubated at 70 °C for 10 minutes) prior to RNA collection using the SV Total RNA Isolation System (Promega Corporation). RT-PCR analysis was performed using the miScript SYBR® Green PCR Kit (Qiagen), following the manufacturer's guidelines. For the present study, the mean quantification cycle (Cq) represents the number of cycles needed to reach a computer-determined fluorescence amplification threshold of approximately 75 times the background (negative control) fluorescence level. Cq values correlate with the relative amount of starting sample, with a lower Cq correlating with a higher amount of starting sample and *vice versa*. Fig. 3b summarizes the RT-PCR results, displaying the mean quantification cycle (Cq) for the target miR-550, in addition to two additional potential targets (miR 1290 and miR 16) as well as the bookkeeping strand RNU 6, confirming the presence of the target miR-550 in the sample, as expected. However, we found that RT-PCR could not be used to quantify SAW lysis because the SAW lysis unit produces ~100 μL of lysed cell media, whereas RT-PCR requires 5–10 mL of sample in order to isolate a sufficient number of exosomes as previously noted.

3.2 SAW-induced exosome lysis characterization

SAW-induced lysing was achieved by exposing raw cell media to ~30 s of SAW at 1 W of power, and the results were quantified using NanoSight nanoparticle tracking measurements. Fig. 4a shows particle size distributions averaged across multiple trials for three sets of experiments: (1) raw cell media, (2) cell media pumped through the channel with the SAW

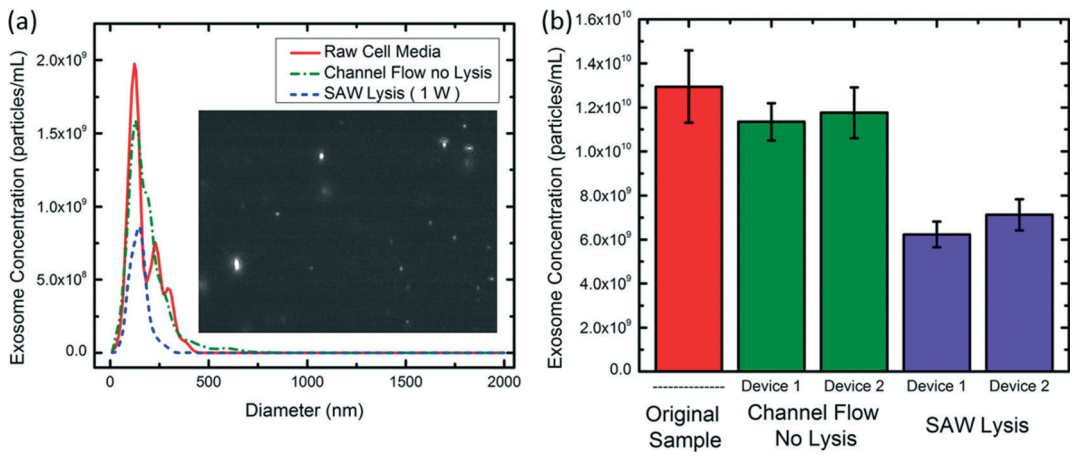

Fig. 4 (a) Average Nanosight LM10 size distributions for exosomes in the cell media sample. While there is a 10.8% loss due to flow in the channel alone (difference between red and green curves), turning on the SAW device decreases the exosome count substantially. The inset shows visual confirmation of exosomes in the cell media obtained from the Nanosight. (b) Quantified exosome concentrations from the size distributions using two separate SAW lysis units, with four samples processed by each. Error bars: 1 standard deviation.

 This journal is © The Royal Society of Chemistry 2015

Published on 11 February 2015. Downloaded by University of Notre Dame on 20/03/2015 19:26:49.

device turned off as a negative control, and (3) cell media pumped through the microfluidic channel while exposed to action of the SAW device. For these experiments, two separate SAW-channel devices were fabricated and four sets of experiments with steps (1) to (3) were conducted on each so that there were 8 measurements of the SAW lysed sample in all. In each experiment, an identical sample volume of 100 μL was collected. Fig. 4b shows the quantified exosome concentration statistics based on the reported Nanosight values. These experiments indicate that 10% of the exosomes are lost when flowing through the microchannel, likely because they stick to the channel walls. Of the remainder, 42% are lysed, for an overall lysis rate of 38 ± 10% (all data are expressed as the mean ± standard deviation). It should be noted that the exosome size distributions shown in TEM images (*e.g.*, Fig. 3a) are generally not comparable to those produced by the Nanosight in part because the TEM analysis particles are dehydrated and observed in vacuum rather than counted *in vivo* as for the Nanosight, which causes shrinkage.[52–54]

While this lysis rate is satisfactory for the present study, it should be noted that significant improvements may be possible. To date, no comprehensive study has been undertaken to study lysis rate as a function of channel height, SAW wavelength, applied power, cell membrane elasticity, fluid properties, or any number of other possible variables. A more thorough understanding of the lysis mechanisms (whether mechanical or electric in nature) should yield improvement. Additional steps may also be taken to prevent loss of exosomes due to the adhesion to the walls of the device. In particular, a number of researchers have had success in preventing the cell and protein adhesion to surfaces *via* chemical treatment of the device walls,[55–57] which suggests a similar approach may prove fruitful for exosome analysis. This approach would not require substantial changes to the fabrication process.

3.3 Nanomembrane sensor calibration

3.3.1 Description of model. Before using our nanomembrane sensor to quantify miR-550 in our raw cell media samples, it was necessary to calibrate it. Fig. 5 shows representative CVC data for one of our nanomembrane sensors before attachment of the complementary probe (baseline), after functionalizing the membrane with the probe (probe) and after hybridizing with the target miR-550 of a various concentrations for 15 min, where the sensor was regenerated after each measurement. The CVCs are acquired by ramping the current at a rate of 0.5 μA s^{-1}. The voltage shift in the over-limiting region is indicative of hybridization and has been associated with vortex suppression by the hybridized probe-target,[35] and progressively higher concentrations of the target on the sensor results in larger voltage shift ΔV until the sensor saturates. Calibration is determined by measuring the ΔV at a pre-defined current in the overlimiting regime and correlating ΔV to the concentration C. The current where these shifts are measured was chosen separately for each

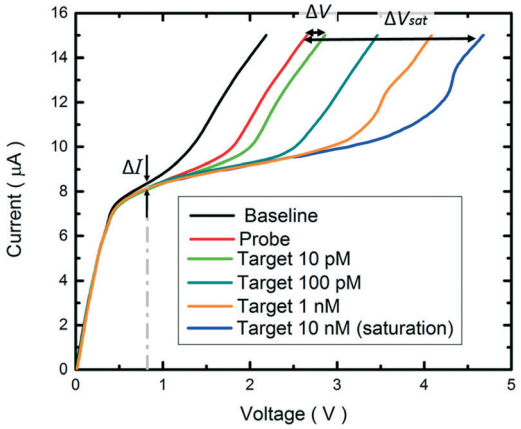

Fig. 5 Representative current voltage characteristic (CVC) for nanomembrance sensor. The black, red, and blue curves indicate a CVC taken with the bare membrane, a CVC taken with the probe attached to the membrane, and a CVC taken with the probes on the membrane surface fully saturated with target RNA, respectively. ΔV measurements were taken at 15 μA, while the limiting current I_o and current shift ΔI were measured at 0.822 V (dotted grey line). Additional CVCs are given in the ESI.†

chip to be as high as possible without damaging the membrane.

In previous work, as many as eight calibration points were needed to detail the full dynamic range of the sensor.[33] However a universal calibration curve valid over the entire range of the sensor significantly expedites the calibration process. To determine a universal calibration curve, we derive a formula that requires only two calibration points to determine two unknown parameters – the saturation voltage shift ΔV_{sat} and the Langmuir equilibrium constant K related to the maximum capacity of the sensor in the linear dynamic range.

The voltage shift we observe in the response of the nanomembrane sensor results from target RNAs binding to complimentary probes on the surface of the membrane. This process may be described using the Langmuir adsorption model,[58,59] which relates the adsorption of molecules on a solid surface to the concentration C of the molecules in the fluid above the solid surface, by using coverage dependent absorption (k_r) and desorption (k_f) rates:

$$k_r\theta = k_f C(1 - \theta), \quad (1)$$

where θ is the fractional coverage of the target on the surface. Rearranging,

$$\theta = \frac{KC}{1 + KC}, \quad (2)$$

where $K = k_f/k_r$ is the affinity or Langmuir equilibrium constant. This parameter describes how strongly the target molecule is attracted to the surface for binding. We see that K has units of inverse concentration, and according to eqn (2) it is related to the critical concentration when exactly half of the target has bound to probes on the membrane (so when $\theta = 1/2$, $K = 1/C_{critical}$). Thus K can also be interpreted as a

Published on 11 February 2015. Downloaded by University of Notre Dame on 20/03/2015 19:26:49.

measure of the target capacity of the sensor within the linear dynamic range.

We may relate θ to the measured voltage ΔV shift by noting that each time a target miRNA reaches a probe and binds, the impedance of the system increases. For ΔV measurements taken at constant current as in Fig. 5, this implies that the voltage will increase proportionally. We thus assume $\theta = \Delta V/\Delta V_{sat}$ so that coverage by the target reduces the ion flux cross-section area and increases the ion-current resistance proportionally until all the probes have hybridized at saturation ΔV_{sat}. Therefore, we have the calibration equation,

$$\frac{\Delta V}{\Delta V_{sat}} = \frac{KC}{1+KC}. \quad (3)$$

While the parameter K is not necessarily known *a priori* and may vary between different membrane sensors, we shall see that it can be extracted from the initial slope of the calibration curve at low concentrations. Expanding eqn (3) in a Taylor series at the low concentration limit, we find that

$$\frac{\Delta V}{\Delta V_{sat}} \approx KC. \quad (4)$$

Taking a derivative of voltage shift with respect to concentration and evaluating at low concentration yields

$$K = \frac{1}{\Delta V_{sat}} \frac{\partial \Delta V}{\partial C}\bigg|_{C=0}. \quad (5)$$

We see that although each membrane sensor device varies in sensitivity due to differences in fabrication and variations in the membrane surface topology, it is possible to construct a universal calibration curve by normalizing voltage and current measurements with the saturation voltage shift ΔV_{sat} and using a critical concentration inversely proportional to K. As previously noted, this reduces the number of calibration points required to two. Experimentally, a calibration curve may be constructed in full by using the zero-shift voltage at zero target concentration and taking a measurement at a relatively low concentration (5 pM) and another measurement at high concentration (100 nM) so that K and ΔV_{sat} may be extracted from the initial slope and the saturation voltage shift.

The theoretical relationship between concentration of target miRNA and voltage shift derived above was verified with data taken from 7 different membrane sensors, normalized using the parameters K and ΔV_{sat} determined separately for each sensor. Data for all 7 sensors are shown in the ESI,† including the currents chosen for each chip where these shifts are measured. The parameter ΔV_{sat} was obtained from one saturation voltage measurement for each sensor at high concentration (10 nM) as previously described. The constant K was obtained by finding the slope between the zero-shift voltage with no target molecules and the voltage shift from one low-concentration (5 pM) measurement to obtain an approximate slope for use in eqn (5). Fig. 6a shows the raw data prior to normalization alongside the Langmuir adsorption calibration curves given by eqn (3) with parameters extracted from two data points as described above. The collapsed normalized data is shown in Fig. 6b. The linear dynamic range spans two decades, computed by fitting a line to the linear and saturation regions of the calibration and measuring the concentration at which they intersect relative to the limit of detection. We observe excellent agreement between theory and experimental data, even though the voltage shifts are measured at different currents, apart from one anomalous data set given by closed red markers in Fig. 6a. In the initial linear region only (not including the saturation region since detection occurs in the initial linear region only), we find a coefficient of determination of $R^2 = 0.88$ excluding this anomalous data set and $R^2 = 0.82$ with the anomalous data set included; both being satisfactory given the potential for variation across sensors. The average limit of detection was computed as 2 pM based upon the mean voltage and standard deviation of four blank measurements taken on each of the seven nanomembrane sensors tested. Large variations were observed in the values for the two parameters, however, with $C_{critical} = 209 \pm 73$ pM (=1/K) without the anomalous data set and $C_{critical} = 184 \pm 94$ pM with it. We find that $\Delta V_{sat} = 0.92 \pm 0.59$ V without the anomalous data set and $\Delta V_{sat} = 0.84 \pm 0.58$ V including it.

3.3.2 *A priori* parameter estimation. In order to further simplify the calibration in future studies, we explore the possibility of estimating the two parameters K and ΔV_{sat} using data available from the CVC of the bare nanomembrane and the CVC of the nanomembrane with only the probe attached, before the system is exposed to the target miRNA. The Langmuir equilibrium constant K, which is dependant on the free energy of absorbance when a target miRNA binds to a probe on the membrane surface, should ideally be the same for all chips whenever the same target/probe pair are used, obviating the measurements at low concentration during calibration that would otherwise be required for every chip. However, as previously mentioned, significant variation occurs in practice, perhaps due to inconsistencies in fabrication or due to variations in the surface energy of the membrane itself. Improvements in the fabrication process for the membrane sensor or use of a different brand of nanoporous membrane may yield more consistent values in future studies, but at the present time it is advisable to take a low concentration measurement for every chip to estimate K, since the parameter K is especially important in defining the low-concentration portion of the calibration curve (Fig. 5b) where measurements will be taken during practical use of the device.

In order to estimate the parameter ΔV_{sat}, we consider the limiting current in both the bare membrane and the membrane with the probe attached. (Note that in this section, the anomalous data set, closed red markers in Fig. 6, is excluded from all calculations.) Previous studies have demonstrated

 This journal is © The Royal Society of Chemistry 2015

Published on 11 February 2015. Downloaded by University of Notre Dame on 20/03/2015 19:26:49.

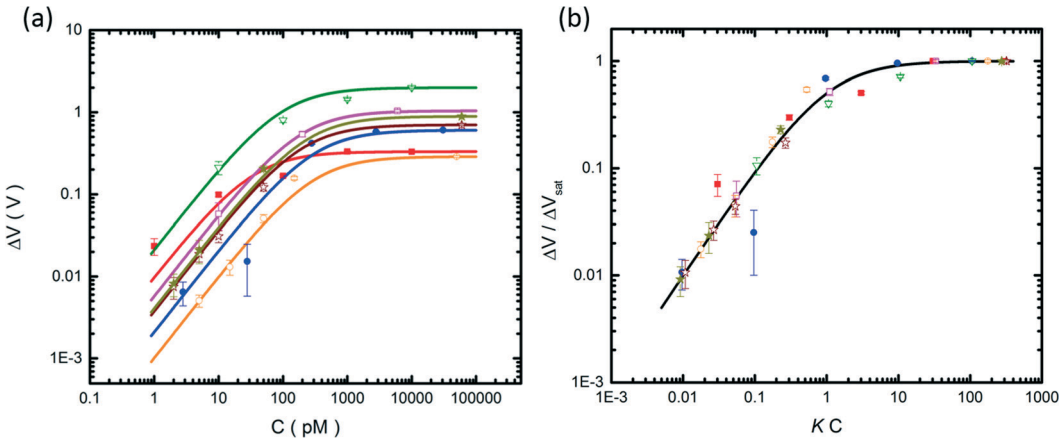

Fig. 6 (a) Voltage shift (ΔV) as a function of the concentration (C) for five separate membrane sensors. Solid lines show the calibration curve eqn (3) with parameters extracted from two data points. (b) Corresponding data normalized by the saturated voltage shift ($\Delta V/\Delta V_{sat}$) as a function of the normalized concentration (KC) for seven separate membrane sensors along with the universal calibration curve from eqn (3). Each data set was normalized by its maximum saturation voltage shift ΔV_{sat} and the affinity constant K determined by the slope of the curve at low concentration, extracted from two data points. Error bars: 1 standard deviation.

that the limiting current is proportional to the area of the membrane.[60] When the probe is attached to the bare membrane, the limiting current is reduced, corresponding to a reduction in the effective area of the membrane due to probes attaching to the surface of the nanoporous membrane and blocking the pore openings. This means that the fractional change in the limiting current, $\Delta I/I_o$, measures the membrane surface area that the probe covers. That is, $\Delta I/I_o = \Delta A/A$, where A is the membrane surface area, I_o is the initial limiting current of the bare membrane, before the probe is applied, and ΔI is measured as the average current shift in the limiting regime as indicated in Fig. 1b, and is hence related to probe density. More specifically, the limiting current region is defined to be the voltage range between the two "knees" of the base-line probe-free bare-membrane CVC curve with maximum curvatures. The average limiting current I_o and current shift ΔI can be accurately estimated by values at the mid-point of this voltage range. The voltage values for each chip where these current shifts are measured as indicated in the ESI.† It is known that probes binding to the surface of the nanoporous membrane also cause the voltage shift ΔV in the overlimiting regime, in this case as a result of the hydrodynamic mechanism of vortex suppression.[33] It is thus unsurprising that $\Delta I/I_o$ correlates with $\Delta V_{sat}/V_o$, where V_o is the voltage in the overlimiting regime before the target is added, with only the probe attached. This relationship is shown in Fig. 7a, along with the linear regression line

$$\Delta V_{sat}/V_o = 15.83(\Delta I/I_o), \quad (6)$$

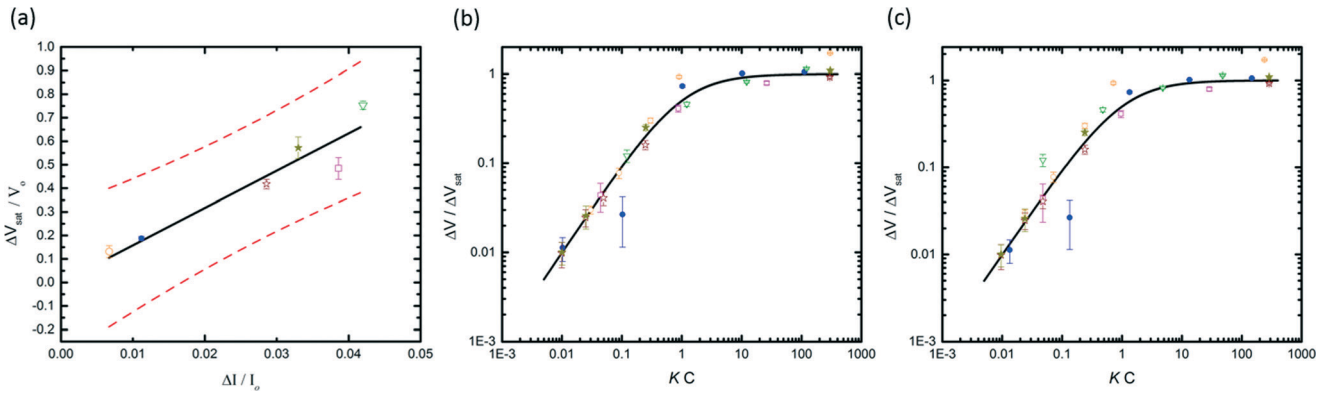

Fig. 7 (a) Correlation between the fractional change in the limiting current ($\Delta I/I_o$) and the fractional change in voltage when the probes on the membrane surface are saturated with target miRNA ($\Delta V_{sat}/V_o$), together with the empirical correlation $\Delta V_{sat}/V_o = 15.83\Delta I/I_o$ marked with a solid black line and 95% confidence interval marked with dotted red lines. (b) Data normalized by the saturated voltage shift ($\Delta V/\Delta V_{sat}$) as a function of the normalized concentration (KC) for five separate membrane sensors along the universal calibration curve from eqn (3). Here, the maximum saturation voltage shift ΔV_{sat} was computed *a priori* from the empirical correlation in (a), while the affinity constant K was determined from one data point using the slope of each calibration at low concentration. (c) Data normalized with ΔV_{sat} computed *a priori* from the empirical correlation in part and K = 1/(209 pM) held constant for all chips. The anomalous data set shown in Fig. 6 in closed red markers is excluded from all parts (a)–(c). Error bars: 1 standard deviation.

Published on 11 February 2015. Downloaded by University of Notre Dame on 20/03/2015 19:26:49.

for the same sensors shown in Fig. 6a. Using eqn (6) to compute ΔV_{sat} (rather than use a measured value of ΔV_{sat}) yields the collapsed normalized data of Fig. 7b with a value of R^2 = 0.78 in the initial linear region only. Collapsing the data using both the voltage correlation and a constant K value for all data sets of $K = 1/C_{critical}$ = 1/209 pM (using $C_{critical}$ = 209 pM for the case where the anomalous data set is excluded) yields the result shown in Fig. 7c with a value of R^2 = 0.72 in the initial linear region. This indicates that reducing the number of calibration points may still yield results accurate enough for some applications, with room for improvement in future work.

3.4 RNA quantification

Detection of the target miRNA contained both in the cell media sample (free floating) and after lysis was performed using the universal calibration curve. We performed detection on two different membrane sensors, using two calibration points on each to obtain K and ΔV_{sat} in combination with the universal calibration curve shown in Fig. 6b. Each cell media sample was placed on the sensor prior to measurement, washed off, and then repeated twice more for a total of three measurements per sample per sensor. Fig. 8 shows that the raw cell media has a concentration of 6 ± 1 pM of free-floating miRNA, while the SAW lysed sample has 13 ± 2 pM. We estimate that this sample of cell media sample contained $8.2 \pm 0.5 \times 10^8$ exosomes mL^{-1}, computed as the average and standard deviation of four subsamples with concentrations reported from the Nanosight according to the protocol described in Section 2.2. Taking into account exosome loss and lysis, we estimate that there are 14 ± 6 copies of the target miRNA 550 per exosome. Use of the *a priori* estimate for ΔV_{sat} (calibration curve Fig. 7b), and the *a priori* estimates for both ΔV_{sat} and K (calibration curve Fig. 7c) yields estimates of 15 ± 6 and 10 ± 9 copies of target RNA per exosome, respectively, which are comparable to the estimate of 14 copies per exosome produced without *a priori* parameter estimation.

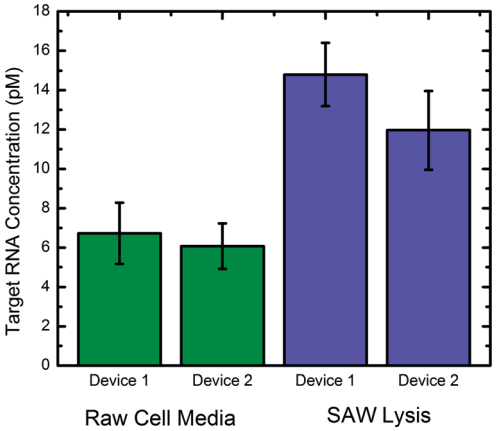

Fig. 8 Target RNA concentration as detected by the nanomembrane sensor and determined using the universal calibration curve before and after SAW lysis for two different nanomembrane devices. Error bars: 1 standard deviation.

These findings are consistent with the findings of others. It is well known that free floating miRNA are stable in cell media independent of exosomes, likely the by-product of dead cells.[61] Furthermore, it has previously been reported that tumour cells have the same concentration of the target miR-550 as the exosomes themselves,[62] so it is unsurprising that this target is found free floating in extracellular space in comparable quantity as within the exosomes themselves. Based on our studies involving cancerous pancreatic cell lines and prior findings by others, we have independent confirmation[63] that there are ~10^3–10^4 highly expressed RNA per exosome and ~10^2–10^3 different genes or miRNA, which implies than an estimate of ~10 target miRNA per exosome is reasonable.[63,64]

Although in the current study the target miR-550 is present within the exosomes as well as free-floating in approximately equal amounts, this will likely not be true for most targets of interest in future studies. For instance, Valadi *et al.* conducted a study on exosomes from the mouse cell line MC/9 and the human cell line HMC-1 that demonstrated that of the 1300 genes present, many were not found in the cytoplasm of the donor cell.[65] A review by Vlassov *et al.* emphasizes that RNA degrades rapidly when in peripheral circulation in blood, and that exosomes provide the necessary protective packaging in this biological fluid.[7] The biological significance of RNA contained within exosomes (as opposed to cellular or free-floating RNA) is underscored by Chen *et al.*, who suggests that the selective enrichment of a group of miRNAs in an exosome sample reveals a "nonrandom but orchestrated network before their release", making it "essential" from a biological perspective to study exosomes and the mechanism by which particular miRNAs are directed to these exosomes.[66] The upshot of these studies is that although the particular target used for the present study was present in appreciable quantities in both free floating media and in the exosomes, a device which lyses exosomes with minimal sample loss or contamination will prove crucial to future studies due to the biological significance of exosomal miRNA in particular and due to the degradation of free floating miRNA free floating in the blood. This will be important in future work on mice models or human-based samples.

4. Conclusions

We have demonstrated SAW-driven exosome lysis coupled with nanomembrane sensor-based microRNA detection as a promising vehicle for the study and early diagnosis of pancreatic cancer. SAW lysis of exosomes was demonstrated for the first time as an on-chip alternative to chemical lysates, which chemically interfere with detection using the nanomembrane sensor. A universal calibration curve was developed for the nanomembrane sensor for miRNA detection and was used to analyse unlysed and lysed samples. These rapid, sensitive, and non-invasive tools provide a new approach to the

 This journal is © The Royal Society of Chemistry 2015

Published on 11 February 2015. Downloaded by University of Notre Dame on 20/03/2015 19:26:49.

diagnosis and prognosis of cancer *via* detection of miRNAs. Taken together, the devices presented here push forward the state of the art in exosome detection and identification.

This study demonstrates the feasibility of microfluidic miRNA profiling for cancer study and diagnosis, paving the way for full integration of the different components onto a single device in the near future. An integrated configuration will eliminate losses of exosomes occurring in sample transfer and allow for automated processing, with both devices both be operated and controlled by the same portable electrical instrument. The integrated device can likely be achieved by attaching an ion-exchange membrane and electrodes to disposable port fittings integrated downstream of the SAW lysis unit, without requiring new advances in microfluidic fabrication techniques. Membrane probes for several different target miRNAs could then be integrated on a single chip with measurements taken in series, so that multiple target miRNAs can be analysed without increasing the duration of the experiment, putting early diagnosis of pancreatic cancer within reach. Blood or other biological samples with greater debris content may be incorporated into the device after additional centrifugation steps or a filter incorporated into the device. Future work should also be conducted to more fully explore SAW lysis with an eye towards optimizing lysis rate as a function of SAW frequency, channel height, and other parameters. Although the current lysis rate is only 38%, significant improvement may be possible without increasing the residence time.

Acknowledgements

The authors wish to acknowledge Professor Jeffrey S. Schorey at the University of Notre Dame for permission to use his Nanosight LM10 and Professor Robert Stahelin at the Indiana University School of Medicine at South Bend for use of his Dynamic Light Scattering (DLS) equipment. In addition, the authors would like to thank Mayra Alejandra Duarte Ow for help in producing the figures. DT is supported by the Harper Cancer Research Institute and the Walther Cancer Foundation.

Notes and references

1 H. Brenner, *Lancet*, 2002, **360**, 1131–1135.
2 A. Osman, *Clin. Lab.*, 2012, **58**, 393–402.
3 A. Ventura and T. Jacks, *Cell*, 2009, **136**, 586–591.
4 W. Stoorvogel, *Blood*, 2012, **119**, 646–648.
5 R. A. Dragovic, C. Gardiner, A. S. Brooks, D. S. Tannetta, D. J. P. Ferguson, P. Hole, B. Carr, C. W. G. Redman, A. L. Harris, P. J. Dobson, P. Harrison and I. L. Sargent, *Nanomed.: Nanotechnol., Biol. Med.*, 2011, 7, 780–788.
6 J. Schageman, E. Zeringer, M. Li, T. Barta, K. Lea, J. Gu, S. Magdaleno, R. Setterquist and A. V. Vlassov, *BioMed Res. Int.*, 2013, **2013**, 253957.
7 A. V. Vlassov, S. Magdaleno, R. Setterquist and R. Conrad, *Biochim. Biophys. Acta, Gen. Subj.*, 2012, **1820**, 940–948.
8 X. Li and M. Donowitz, in *Exocytosis and Endocytosis*, ed. A. Ivanov, Humana Press, 2008, ch. 8, vol. 440, pp. 97–110.
9 B. J. Tauro, D. W. Greening, R. A. Mathias, H. Ji, S. Mathivanan, A. M. Scott and R. J. Simpson, *Methods*, 2012, **56**, 293–304.
10 C. Sser, M. Eldh and J. Tvall, *Isolation and Characterization of RNA-Containing Exosomes*, 2012, p. e3037.
11 G. Lami, M. R. Biagini and A. Galli, *World J. Gastroenterol.*, 2014, **6**, 272.
12 A. Garuti, I. Rocco, G. Cirmena, M. Chiaramondia, P. Baccini, M. Calabrese, C. Palermo, D. Friedman, G. Zoppoli and A. Ballestrero, *Gynecol. Oncol.*, 2014, **132**, 389–396.
13 D. Morgan, *Surface Acoustic Wave Filters, With Applications to Electronic Communications and Signal Processing*, Academic Press, Waltham, Massachusetts, 2nd edn, 2007.
14 B. A. Auld, *Acoustic Fields and Waves in Solids*, Krieger Publishing Company, Malabar, Florida, 1990.
15 J. Ho, M. K. Tan, D. B. Go, L. Y. Yeo, J. R. Friend and H.-C. Chang, *Anal. Chem.*, 2011, **83**, 3260–3266.
16 M. K. Tan, J. R. Friend and L. Y. Yeo, *Lab Chip*, 2007, 7, 618–625.
17 D. P. Morgan, *Int. J. High Speed Electron. Syst.*, 2000, **10**, 553–602.
18 W.-K. Tseng, J.-L. Lin, W.-C. Sung, S.-H. Chen and G.-B. Lee, *J. Micromech. Microeng.*, 2006, **16**, 539.
19 D. Taller, D. B. Go and H.-C. Chang, *Phys. Rev. Lett.*, 2012, **109**, 224301.
20 H. Li, J. Friend and L. Yeo, *Biomed. Microdevices*, 2007, **9**, 647–656.
21 P. R. Rogers, J. R. Friend and L. Y. Yeo, *Lab Chip*, 2010, **10**, 2979–2985.
22 S. R. Heron, R. Wilson, S. A. Shaffer, D. R. Goodlett and J. M. Cooper, *Anal. Chem.*, 2010, **82**, 3985–3989.
23 J. Reboud, Y. Bourquin, R. Wilson, G. S. Pall, M. Jiwaji, A. R. Pitt, A. Graham, A. P. Waters and J. M. Cooper, *Proc. Natl. Acad. Sci. U. S. A.*, 2012, **109**, 15162–15167.
24 T. J. Lyford, P. J. Millard and M. P. da Cunha, *Cell lysisa using surface acoustic wave devices for sensor applications*, 2012.
25 X. Ding, P. Li, S.-C. S. Lin, Z. S. Stratton, N. Nama, F. Guo, D. Slotcavage, X. Mao, J. Shi, F. Costanzo and T. J. Huang, *Lab Chip*, 2013, **13**, 3626–3649.
26 Y. Chen, X. Ding, S.-C. Steven Lin, S. Yang, P.-H. Huang, N. Nama, Y. Zhao, A. A. Nawaz, F. Guo and W. Wang, *ACS Nano*, 2013, **7**, 3306–3314.
27 F. Guo, P. Li, J. B. French, Z. Mao, H. Zhao, S. Li, N. Nama, J. R. Fick, S. J. Benkovic and T. J. Huang, *Proc. Natl. Acad. Sci. U. S. A.*, 2015, **112**, 43–48.
28 X. Ding, S.-C. S. Lin, B. Kiraly, H. Yue, S. Li, I.-K. Chiang, J. Shi, S. J. Benkovic and T. J. Huang, *Proc. Natl. Acad. Sci. U. S. A.*, 2012, **109**, 11105–11109.
29 A. de Gassart, C. Géminard, B. Février, G. Raposo and M. Vidal, *Blood*, 2003, **102**, 4336–4344.
30 I. Feliciello and G. Chinali, *Anal. Biochem.*, 1993, **212**, 394–401.
31 J. P. Banáth, A. Kim and P. L. Olive, *Radiat. Res.*, 2001, **155**, 564–571.
32 Z. Slouka, S. Senapati and H.-C. Chang, *Annu. Rev. Anal. Chem.*, 2013, 317–335.

Published on 11 February 2015. Downloaded by University of Notre Dame on 20/03/2015 19:26:49.

33 Z. Slouka, S. Senapati, Y. Yan and H.-C. Chang, *Langmuir*, 2013, **29**, 8275–8283.
34 S. Senapati, Z. Slouka, S. S. Shah, S. K. Behura, Z. Shi, M. S. Stack, D. W. Severson and H.-C. Chang, *Biosens. Bioelectron.*, 2014, **60**, 92–100.
35 G. Yossifon, P. Mushenheim, Y.-C. Chang and H.-C. Chang, *Phys. Rev. E: Stat., Nonlinear, Soft Matter Phys.*, 2009, **79**, 046305.
36 I. Rubinstein and L. Shtilman, *J. Chem. Soc., Faraday Trans. 2*, 1979, **75**, 231–246.
37 A. Li, J. Yu, H. Kim, C. L. Wolfgang, M. I. Canto, R. H. Hruban and M. Goggins, *Clin. Cancer Res.*, 2013, **19**, 3600–3610.
38 C. S. Hartmann and B. P. Abbott, *Overview of design challenges for single phase unidirectional SAW filters*, 1989.
39 T. Kodama, H. Kawabata, H. Sato and Y. Yasuhara, *Electronics and Communications in Japan (Part II: Electronics)*, 1987, **70**, 32–44.
40 H. Nakamura, T. Yamada, T. Ishizaki and K. Nishimura, *IEEE Trans. Microwave Theory Tech.*, 2001, **49**, 761–768.
41 R. Shilton, M. K. Tan, L. Y. Yeo and J. R. Friend, *J. Appl. Phys.*, 2008, **104**, 014910.
42 A. Qi, L. Yeo, J. Friend and J. Ho, *Lab Chip*, 2010, **10**, 470–476.
43 V. Filipe, A. Hawe and W. Jiskoot, *Pharm. Res.*, 2010, **27**, 796–810.
44 A. Malloy, *Mater. Today*, 2011, **14**, 170–173.
45 L. Alvarez-Erviti, Y. Seow, H. Yin, C. Betts, S. Lakhal and M. J. Wood, *Nat. Biotechnol.*, 2011, **29**, 341–345.
46 A.-K. Ludwig and B. Giebel, *Int. J. Biochem. Cell Biol.*, 2012, **44**, 11–15.
47 P. P. Singh, V. L. Smith, P. C. Karakousis and J. S. Schorey, *J. Immunol.*, 2012, **189**, 777–785.
48 J. Caradec, G. Kharmate, E. Hosseini-Beheshti, H. Adomat, M. Gleave and E. Guns, *Clin. Biochem.*, 2014, **47**, 1286–1292.
49 C. Redman, D. Tannetta, R. Dragovic, C. Gardiner, J. Southcombe, G. Collett and I. Sargent, *Placenta*, 2012, **33**, S48–S54.
50 Y. Ouyang, J.-F. Mouillet, C. Coyne and Y. Sadovsky, *Placenta*, 2014, **35**, S69–S73.
51 M. Kesimer, M. Scull, B. Brighton, G. DeMaria, K. Burns, W. O'Neal, R. J. Pickles and J. K. Sheehan, *FASEB J.*, 2009, **23**, 1858–1868.
52 O. Jensen, J. Prause and H. Laursen, *Albrecht von Graefes Arch. Klin. Exp. Ophthalmol.*, 1981, **215**, 233–242.
53 C. Théry, S. Amigorena, G. Raposo and A. Clayton, *Current Protocols in Cell Biology*, 2006, pp. 3.22. 21–23.22. 29.
54 Y. Yuana, R. M. Bertina and S. Osanto, *Thromb. Haemostasis*, 2011, **105**, 396.
55 D. W. Inglis, R. Riehn, R. Austin and J. Sturm, *Appl. Phys. Lett.*, 2004, **85**, 5093–5095.
56 N. F. Owens, D. Gingell and P. R. Rutter, *J. Cell Sci.*, 1987, **87**, 667–675.
57 T. McPherson, A. Kidane, I. Szleifer and K. Park, *Langmuir*, 1998, **14**, 176–186.
58 D. D. Do, *Adsorption analysis*, World Scientific, 1998.
59 F. L. Slejko, *Adsorption technology. A step-by-step approach to process evaluation and application*, Dekker, New York, Basel, 1985.
60 H.-C. Chang and L. Y. Yeo, *Electrokinetically driven microfluidics and nanofluidics*, Cambridge University Press, Cambridge, UK, 2010.
61 A. Turchinovich, L. Weiz, A. Langheinz and B. Burwinkel, *Nucleic Acids Res.*, 2011, **39**(16), 7223–7233.
62 D. D. Taylor and C. Gercel-Taylor, *Gynecol. Oncol.*, 2008, **110**, 13–21.
63 W. W. Chen, L. Balaj, L. M. Liau, M. L. Samuels, S. K. Kotsopoulos, C. A. Maguire, L. LoGuidice, H. Soto, M. Garrett and L. D. Zhu, *Mol. Ther.–Nucleic Acids*, 2013, **2**, e109.
64 S. Keller, J. Ridinger, A.-K. Rupp, J. Janssen and P. Altevogt, *J. Transl. Med.*, 2011, **9**, 86.
65 H. Valadi, K. Ekström, A. Bossios, M. Sjöstrand, J. J. Lee and J. O. Lötvall, *Nat. Cell Biol.*, 2007, **9**, 654–659.
66 W.-X. Chen, Y.-Q. Cai, M.-M. Lv, L. Chen, S.-L. Zhong, T.-F. Ma, J.-H. Zhao and J.-H. Tang, *Tumor Biol.*, 2014, 1–11.

 This journal is © The Royal Society of Chemistry 2015